Cosmological Implications of First-Order Phase Transitions

Thomas Konstandin[1], *Günter Sigl*[2]

[1]DESY, Hamburg, Germany
[2]II. Institut für Theoretische Physik, Universität Hamburg, Germany

DOI: http://dx.doi.org/10.3204/PUBDB-2018-00782/C10

Phase transitions in the early Universe can lead to many potentially observable effects such as the generation of primordial magnetic seed fields, gravitational waves and baryon- and lepton number. They depend on yet not well known properties, such as the order of the phase transitions, that can be influenced by physics beyond the Standard Model.

1 Introduction

Project C10 of the SFB 676 is concerned with cosmological implications of first-order phase transitions. The appeal of cosmological phase transitions is that they provide a link between cosmological observations and the energy frontier of particle physics. As an analogy consider the cosmic microwave background (CMB). The observations of the CMB are very predictive because we understand atomic physics well from the laboratory experiments. Image we would have observed the CMB without the detailed knowledge on atomic physics. Ultimately, we could use the CMB data to learn something about the physics of the hydrogen atom. This is basically the situation with the electroweak phase transition. In case it is first order – which depends on the scalar sector of the particle physics theory – many interesting phenomena result that can teach us about particle physics on electroweak energy scales.

The project C10 deals with a variety of aspects of cosmological phase transition. This includes understanding the nature of the phase transition and its properties in various extensions of the Standard Model (SM). The trademark of first-order phase transitions (1st-order PTs) is that they proceed by bubble nucleation. The prime example for this kind of phase transition is boiling water – where bubbles of gas expand into the liquid phase – or chemical combustion where a fireball rapidly consumes all its surroundings. Important characteristics are the latent heat that is released by the phase transition into the plasma or the velocity with which the phase boundary is moving. Part of C10 is concerned with developing tools to assess these characteristics in an efficient way.

Another aspect of C10 is model building. Particle physics models are currently tested by the LHC experiments at CERN which allows to cross-correlate the knowledge from colliders that is relevant for the electroweak phase transition with cosmological observations. For example, additional bosonic degrees of freedom (that might be strongly coupled to the Higgs particle) have a strong impact on the electroweak phase transition. The discovery of an extended scalar sector would hence have far-reaching implications also in cosmology.

Various subfields of physics meet at the theory of cosmological phase transitions, in particular particle physics, thermodynamics and magnetohydrodynamics. A particular example that played a role in C10 is that fact that a chiral asymmetry in the lepton sector can be transformed into helical magnetic fields under certain circumstances. Since electroweak interactions in particular in the broken phase do violate chiral symmetry, this effect, which is known as the chiral magnetic effect, may contribute to or influence magnetogenesis around the electroweak phase transition.

With the observation of the first gravitational waves from binary mergers by LIGO and VIRGO (see, e.g. Ref. [1] for a binary black hole merger and Ref. [2] for a binary neutron star merger), the era of gravitational wave astronomy began. Also 1st-order phase transitions are a potential source of gravitational waves. The nucleated bubbles collide at the end of the phase transition what leads to gravitational wave production. However, the main source of gravitational waves in this context are actually secondary effects. This includes sound waves in the plasma or hydromagnetic turbulence, which both are a consequence of the phase transition. We performed studies quantifying these phenomena within project C10.

Finally, cosmological 1st-order phase transitions can also explain the observed asymmetry between matter and anti-matter via electroweak baryogenesis. The main advantage of electroweak baryogenesis is that all ingredients required for baryogenesis (mostly CP violation and a departure from equilibrium) result from physics that is testable in the laboratory in the near future. Since baryogenesis requires a potent source of CP violation, an additional strong link to particle physics is present in this context.

In the following sections, we discuss these topics in a little bit more detail and in particular the new results achieved within the project C10.

2 The electroweak phase transition

The main tool to study phase transitions and spontaneous symmetry breaking is the effective action [4]. On a technical level, the effective action is so powerful because it resums so-called tadpole diagrams that show up in conventional perturbative expansions.

Still, the evaluation of the effective action is typically performed in a perturbative way (albeit expanding around the broken vacuum). In many cases, the effective action obtained this way suffers from several shortcomings and often these issues are related to the gauge chosen. One common gauge is the Landau gauge. This gauge has the advantage that the ghost degrees of freedom (mostly) decouple. At the same time, the Goldstone bosons are massless in the broken phase in this gauge. This leads to the fact that infrared (IR) enhanced contributions to the effective action can spoil the convergence of the perturbative expansion. In Refs. [5] and [6], members of C10 analyze the impact of these IR issues in the SM potential and propose a general method to resum the offending terms into an IR safe effective potential.

Since this IR issue seems to be a peculiarity of the Landau gauge, the gauge-dependence of the effective action and observables derived from it is the next obvious question. In a series of papers [3, 7, 8], the gauge dependence of the effective action and the resulting phase transition characteristics were studied. The gauge-dependence is in this context a tricky issue, since the effective action depends on the gauge while observables generally don't. For example, Figure 1 shows the Higgs configuration that leads to vacuum decay, calculated in two different gauges (R_ξ-gauge with $\xi = 0$ and $\xi = 200$). The configurations obey different boundary conditions and carry different kinetic and potential energies. In the end, all these effects conspire to yield

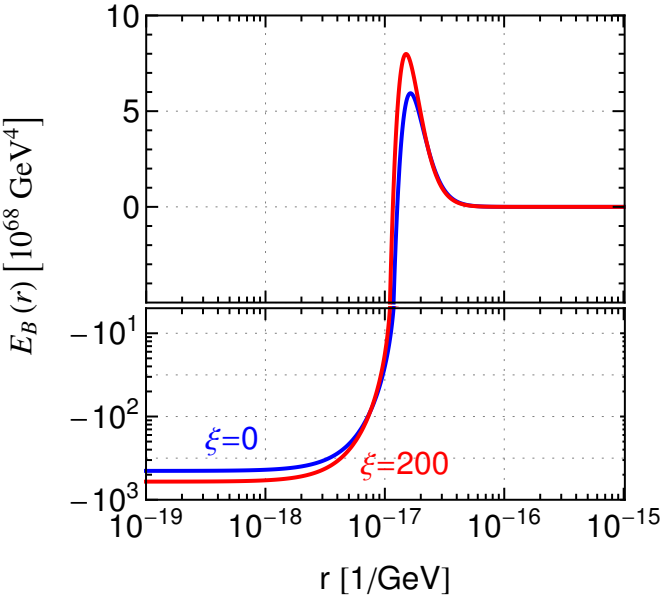

Figure 1: Higgs field configurations that lead to vacuum decay, calculated in two different gauges (R_ξ-gauge with $\xi = 0$ and $\xi = 200$). Figure taken from Ref. [3].

the same (measurable) decay rate.

Another item that is relevant for gravitational wave detection (see sec. 5) and baryogenesis (see sec. 6) are the characteristics of the phase transition. While many properties of the phase transition – as the latent heat or the phase transition temperature – can be readily inferred from the effective potential, some properties require additional work. This is the case for the expansion velocity of the nucleated bubbles during a 1st-order phase transition. The expansion velocity depends on friction which is an out-of-equilibrium phenomenon. Accordingly, one has to grasp the out-of-equilibrium nature of the plasma during the phase transition, which can be tracked using Boltzmann equations. Based on the seminal work by Moore and Prokopec in the SM [9], members of C10 extended the friction calculation to a large variety of models [10].

Another aspect of the electroweak phase transition constitutes model building. Many models beyond the Standard Model that display a strong 1st-order PT, but not all are equally interesting. One guiding principle for model building is minimality. Adding solely a scalar boson or a second Higgs doublet extends the SM particle content marginally while allowing for the rich phenomenology of a 1st-order phase transition [11, 12]. A novel avenue is hereby to connect the phase transition to the flavor puzzle in the Standard Model. The Yukawa couplings of the SM that generate the fermion masses via spontaneous symmetry breaking, span many orders of magnitude in the quark and lepton sector. One way to explain these greatly different coupling constants is to resort to an additional quantum number, a Froggatt–Nielsen charge. Light particles carry larger amounts of this charge leading to smaller couplings. If every additional charge suppresses the coupling by a factor of order one (let's say 10), relatively small quantum numbers can explain the vast hierarchy between the fermion masses. This idea is realized in

the Froggatt–Nielsen mechanism. The novel approach of Ref. [13] connects the mechanism by Froggatt and Nielsen to electroweak symmetry breaking. This greatly enhances the strength of the phase transition and leads to new sources of CP violation as required by baryogenesis. We will come back to this question in sec. 6.

3 The chiral magnetic effect: generalities

In project C10 we also have investigated the chiral magnetic effect in particular in the context of the early Universe [14,15]. This effect connects the subjects of magnetohydrodynamics with particle physics, in particular the so-called chiral anomaly, i.e. the non-conservation of chiral lepton currents. Here we discuss general aspects and their relevance in the cosmological context. In the report for project C9 we discuss the chiral magnetic effect in a qualitative way and briefly discuss its role in the context of hot neutron stars.

For the electron chiral asymmetry $N_5 \equiv N_L - N_R$ and the magnetic helicity $\mathcal{H} \equiv \int d^3\mathbf{r}\, \mathbf{B}\cdot\mathbf{A}$ the electromagnetic chiral anomaly gives

$$\frac{d}{dt}\left(N_5 - \frac{e^2}{4\pi^2}\mathcal{H}\right) = 0\,, \tag{1}$$

and $e^2\mathcal{H}/(4\pi^2)$ is just the Chern–Simons number of the electromagnetic field. The generalized Maxwell–Ampère law

$$\boldsymbol{\nabla}\times\mathbf{B} = \frac{\partial\mathbf{E}}{\partial t} + \mu_0\left(\mathbf{j}_{\rm em} + \mathbf{j}_{cB}\right)\,, \quad \text{with} \quad \mathbf{j}_{cB} = -\frac{e^2}{2\pi^2}\mu_5\mathbf{B}\,, \tag{2}$$

and in the absence of external currents Ohm's law $\mathbf{j}_{\rm em} = \sigma\mathbf{E}$ gives

$$\mathbf{E} \simeq -\mathbf{v}\times\mathbf{B} + \eta\left(\boldsymbol{\nabla}\times\mathbf{B} + \frac{2e^2}{\pi}\mu_5\mathbf{B}\right)\,, \tag{3}$$

where $\eta = 1/(\mu_0\sigma)$ is the resistivity and the effective chemical potential is given by

$$\mu_5 = \frac{\mu_L - \mu_R}{2} - V_5 = \frac{\mu_L - V_L - \mu_R + V_R}{2}\,, \tag{4}$$

where V_5 is a possible effective potential due to a different forward scattering amplitude for left- and right-chiral electrons. Inserting this into the induction equation the MHD is modified to

$$\partial_t\mathbf{B} = \boldsymbol{\nabla}\times(\mathbf{v}\times\mathbf{B}) + \eta\Delta\mathbf{B} - \frac{2e^2}{\pi}\eta\mu_5\boldsymbol{\nabla}\times\mathbf{B}\,. \tag{5}$$

This equation is similar to the mean field dynamo equation which also has growing solutions. Neglecting the velocity term the evolution equations for the power spectra M_k and H_k [note $U_B = \int d\ln k M_k$ and $\mathcal{H} = \int d\ln k H_k$] now become

$$\begin{aligned}\partial_t M_k &= -\eta k^2\left(2M_k + \frac{e^2}{2\pi^2}\mu_5 H_k\right)\,,\\ \partial_t H_k &= -\eta\left(2k^2 H_k + 32e^2\mu_5 M_k\right)\,.\end{aligned} \tag{6}$$

Integrating over $\ln k$ gives

$$\partial_t \mathcal{H} = -\eta \int d\ln k \left(2k^2 H_k + 32e^2 \mu_5 M_k\right) . \tag{7}$$

In an FLRW metric these are comoving quantities and conformal time.

Now express N_5 in terms of μ_5,

$$N_5 = c(T,\mu_e) V \mu_5 , \quad \text{with} \quad c(T,\mu_e) = \frac{\mu_e^2}{\pi^2} + \frac{T^2}{3} \quad \text{for } \mu_e^2 + T^2 \gg m_e^2 , \tag{8}$$

where the second expression holds for relativistic electrons. Applying this to Eq. (1) we get

$$d\mathcal{H} = \frac{4\pi^2}{e^2} dN_5 = \frac{4\pi^2 V c(T,\mu_e)}{e^2} d\mu_5 . \tag{9}$$

We now take into account damping of μ_5 from *chirality flips*. In the cosmological context after electroweak breaking at $T = T_{\rm ew} \simeq 160\,\text{GeV}$ the rate is

$$R_f \simeq \left(\frac{m_e}{6T}\right)^2 R \sim \left(\frac{m_e}{6T}\right)^2 400 \left(\frac{\alpha_{\rm em}}{6T}\right)^2 10\,T^3 \sim 10^{-4} \frac{m_e^2}{T} , \quad T \lesssim T_{\rm ew} , \tag{10}$$

which is larger than the Hubble rate. Before electroweak breaking

$$R_f \simeq \frac{T_5}{T} H(T_5) , \quad T \gtrsim T_{\rm ew} , \quad T_5 \simeq 10\,\text{TeV} . \tag{11}$$

Inserting Eq. (7) into Eq. (9) then yields

$$\partial_t \mu_5 = -\frac{e^2 \eta}{2\pi^2 V c(T,\mu_e)} \int d\ln k \left(k^2 H_k + 16 e^2 \mu_5 M_k\right) - 2R_f \left(\mu_5 - \mu_{5,b}\right) . \tag{12}$$

Here $\mu_{5,b} = -V_5 + \mu_s$ is the equilibrium value of the effective chemical potential μ_5 for $\eta \to 0$. Other processes such as electroweak interactions with other species as for example neutrinos can be taken into account by the term $\mu_{5,b}$ and thus the source term $2R_f\mu_s$.

From Eq. (6) growing solutions exist for wavenumbers

$$k < k_5 \equiv k_5(\mu_5) \equiv \frac{2e^2}{\pi} |\mu_5| . \tag{13}$$

This follows from using helicity modes in Eq. (5) which gives

$$\partial_t b_{\mathbf{k}}^{\pm} = \eta k \left(\mp \frac{2e^2}{\pi} \mu_5 - k\right) b_{\mathbf{k}}^{\pm} , \tag{14}$$

Thus if the condition Eq. (13) is fulfilled, the helicity with the opposite sign as μ_5 will grow whereas the same sign helicity will decay and the absolute value of the helicity will be close to the maximal value given by

$$|H_k| \le \frac{8\pi M_k}{k} . \tag{15}$$

In contrast, for $k \gtrsim k_5$ both helicities will decay with roughly the resistive rate. For the helicity with opposite sign to μ_5 the first term in Eq. (14) corresponds to a growth rate in the cosmological context

$$R_c(k) = \frac{2e^2}{\pi}\eta k|\mu_5| \simeq 2\times 10^{10}\left(\frac{\mathrm{TeV}}{T}\right)\left(\frac{k}{k_5}\right)\left(\frac{\mu_5}{T}\right)^2 H(T)\,, \tag{16}$$

The total rate $R_c - R_r$ reaches its maximum value $R_{\max} = \eta k_5^2/4$ at $k = k_5/2$ which for

$$\frac{\mu_5}{T} \gtrsim 10^{-5}\left(\frac{T}{\mathrm{TeV}}\right)^{1/2} \tag{17}$$

is larger than the Hubble rate. Furthermore, Eq. (12) shows that for growing modes $|\mu_5|$ shrinks for either sign of μ_5. Therefore, the **chiral magnetic instability transforms energy in the electron asymmetry N_5 into magnetic energy**. This is because by definition of the chemical potential μ_5 the energy U_5 associated with the chiral lepton asymmetry is given by

$$dU_5 = \mu_5 dN_5 = Vc(T,\mu_e)\mu_5 d\mu_5\,, \quad U_5 = \frac{Vc(T,\mu_e)\mu_5^2}{2}\,. \tag{18}$$

Now assume that initially $\mu_5 = \mu_{5,i}$ and $U_B = 0$. Since the sign of $d\mu_5$ is opposite to the sign of $\mu_{5,i}$, Eq. (9) implies that the magnetic helicity will have the opposite sign as $\mu_{5,i}$. The growth rate peaks at wavenumber $k = k_5/2$ given by Eq. (13) and for a given mode k growth stops once $|\mu_5|$ has decreased to the point that Eq. (13) is violated. Since the instability produces maximally helical fields saturating Eq. (15), with Eq. (9) we obtain

$$\begin{aligned} dU_B &\simeq dM_{k_5} \simeq k_5|dH_{k_5}|/(8\pi) \simeq k_5|d\mathcal{H}|/(8\pi) = Vc(T,\mu_e)\mu_5 d\mu_5\,,\\ \Delta E_m &\simeq \frac{Vc(T,\mu_e)(\mu_{5,i}^2-\mu_5^2)}{2}\,. \end{aligned} \tag{19}$$

Adding Eqs. (18) and (19) gives a total energy $U_{\mathrm{tot}} = U_5 + U_B \simeq Vc(T,\mu_e)\mu_{5,i}^2/2$ which only depends on $\mu_{5,i}$. The maximal magnetic energy density then becomes

$$\frac{\Delta U_B}{V} \lesssim \frac{c(T,\mu_e)\mu_{5,i}^2}{2} \simeq \frac{\mu_{5,i}^2 T^2}{6}\,, \tag{20}$$

where the last expression follows from Eq. (8). Eq. (12) implies that $\partial_t\mu_5 = 0$ if

$$\tilde{\mu}_5 = \frac{R_f\mu_{5,b} - \frac{2e^2\eta}{\pi c(T,\mu_e)}\int d\ln k k\frac{M_k}{V}\left(\frac{H_k}{8\pi M_k/k}\right)}{R_f + \frac{4e^4\eta}{\pi^2 c(T,\mu_e)}\frac{U_B}{V}}\,, \tag{21}$$

where H_k has again be normalized to its maximal value given by Eq. (15). For negligible magnetic fields $\tilde{\mu}_5 \simeq \mu_{5,b}$, as expected and magnetic field modes with $k < k_5(\mu_{5,b})$ are growing exponentially with rate $R_c(k) - R_r$ given by Eq. (16). The magnetic field terms start to dominate for

$$\frac{U_B}{V} \gtrsim \frac{c(T,\mu_e)R_f}{4e^4\eta} \simeq \frac{10\pi}{3e^4}T^2 m_e^2 \simeq 2\times 10^5 T^2 m_e^2\,, \tag{22}$$

In this case Eq. (21) gives

$$\tilde{\mu}_5 \simeq -\frac{\pi}{2e^2 U_B}\int d\ln k k M_k\left(\frac{H_k}{8\pi M_k/k}\right)\,. \tag{23}$$

This is what in Ref. [16] was discussed as a so-called *tracking solution*. Note that $\tilde{\mu}_5$ from Eq. (21) varies with rates in general much slower than R_f and R_c. Also, since in general $\tilde{\mu}_5 \neq \mu_{5,b}$, the two terms in Eq. (12) do not vanish separately but only tend to compensate each other and are both roughly constant since μ_5 is approximately constant. Since at saturation, Eq. (23), the first term in Eq. (12) vanishes. Thus μ_5 and due to Eqs. (9) also the magnetic helicity change linearly in time with

$$\partial_t \mathcal{H} \simeq \frac{8\pi^2 V c(T,\mu_e)}{e^2} R_f (\mu_5 - \mu_{5,b})\,. \tag{24}$$

Since helicity is nearly maximal this also implies that the magnetic energy also roughly grows or decreases linearly with time, depending on the sign of $(\mu_5 - \mu_{5,b})/\mathcal{H}$.

Combining Eqs. (6), (12) and (18) the rate of change of the total energy is

$$\begin{aligned} \partial_t U_{\rm tot} &= \partial_t U_B + \partial_t U_5 = \\ &= -2\eta \int d\ln k M_k \left\{ (k-k_5)^2 + 2k_5 k \left[\left(\frac{H_k}{8\pi M_k/k} \right) \mathrm{sign}(\mu_5) + 1 \right] \right\} \\ &\quad -2R_f V c(T,\mu_e)\mu_5 \left(\mu_5 - \mu_{5,b}\right)\,, \end{aligned} \tag{25}$$

where $k_5 = k_5(\mu_5)$ is given by Eq. (13). Since the expression in large braces is non-negative due to Eq. (15), up to the term proportional to $\mu_{5,b}$ which describes a possible energy exchange with external particles, the total energy can only decrease due to the finite resistivity and the chirality-flip rate. The only equilibrium state with $\partial_t U_{\rm tot} = 0$ is given by $\mu_5 = \mu_{5,b}$ and a magnetic energy concentrated in the mode $k = k_0 = k_5(\mu_{5,b})$ with maximal magnetic helicity with the opposite sign as $\mu_{5,b}$, $H_{k_0} = \mathrm{sign}(\mu_{5,b}) 8\pi M_{k_0}/k_0$.

The evolution of $\mu_{5,b}$ due to energy exchange with the background matter can be modeled as follows: In absence of magnetic fields multiplying Eq. (12) with $c(T,\mu_e)$ and using Eq. (8) gives

$$\partial_t n_5 = -2R_f [n_5 - c(T,\mu_e)\mu_{5,b}] = \pm R_w n_b - 2R_f n_5\,, \tag{26}$$

where the gain term was written as a parity breaking electroweak rate R_w times the number density n_b of the background lepton species. This implies

$$n_b = 2c(T,\mu_e)\frac{R_f}{R_w}|\mu_{5,b}|\,, \quad \frac{|\mu_{5,b}|}{T} \simeq 0.1 g_b \frac{R_w}{R_f}\,, \tag{27}$$

where the second expression holds for g_b non-degenerate relativistic fermionic degrees of freedom. The energy U_b associated with these background particles is thus given by

$$\frac{U_b}{V} = \int_0^{\mu_{5,b}} \mu'_{5,b} dn_b = \frac{R_f}{R_w} c(T,\mu_e)\mu_{5,b}^2 \sim 3\times 10^{-3} g_b^2 \frac{R_w}{R_f} T^4\,, \tag{28}$$

where the last expression again holds in the non-degenerate relativistic case. Note that for $\mu_{5,i} \sim \mu_{5,b} \sim (R_w/R_f)T$ Eq. (28) is of order $(R_w/R_f)T^4$ whereas U_5 from Eq. (18) is of order $(R_w/R_f)^2 T^4$. Both energies vanish in the limit of parity conservation, $R_w \to 0$, as it should be. In terms of initial equilibrium chiral potential $\mu_{5,bi}$ and for $R_w \lesssim R_f$ the maximal magnetic energy is then

$$\frac{\Delta U_B}{V} \lesssim \frac{R_f}{R_w} c(T,\mu_e)\mu_{5,bi}^2 \sim 3\times 10^{-3} g_b^2 \frac{R_w}{R_f} T^4\,. \tag{29}$$

Setting $\partial_t U_b = -\partial_t U_5$ to conserve energy and equating $\partial_t U_5$ with the last term in Eq. (25) yields an equation for the evolution of $\mu_{5,b}$,

$$\partial_t \mu_{5,b} = R_w \frac{\mu_5}{\mu_{5,b}} (\mu_5 - \mu_{5,b}) \,. \tag{30}$$

When U_b is included in $U_{\rm tot}$ the second term in Eq. (25) is absent in the time derivative of $U_{\rm tot}$. The total energy is then dissipated exclusively through resistive magnetic field damping. Eq. (30) indicates that $\mu_{5,b}$ typically changes with the rate R_w. A stationary state is reached if $\mu_{5,b} = \mu_5$ and the magnetic field concentrates in $k_5 = k_5(\mu_{5,b})$ with maximal helicity of sign opposite to $\mu_{5,b}$. This requires magnetic field growth rates larger than the Hubble rate, see Eq. (17).

The chemical potential μ_5 is continuously recreated with a rate $R_f \mu_{5,b} \sim 0.1 g_b R_w T$, see Eq. (27), and a time-independent or slowly varying μ_5 can be established which is given by Eq. (21). This can be the case, for example, in a supernova or a neutron star due to URCA processes which absorb left-chiral electrons with a rate R_w and turn them into neutrinos that subsequently escape the star.

Due to Eq. (6) amplification stops and resistive damping sets in when $2\eta k_5^2 t \sim 1$, thus

$$k_5 \sim k_5^0 \left(\frac{t_0}{t}\right)^{1/2} , \quad \mu_5 \sim \mu_5^0 \left(\frac{t_0}{t}\right)^{1/2} . \tag{31}$$

4 The chiral magnetic effect in the presence of turbulent velocity fields

In the drag time approximation the Lorentz force induces a velocity

$$\mathbf{v} \sim \tau_d \frac{\mathbf{j} \times \mathbf{B}}{p + \rho} = \tau_d \frac{(\boldsymbol{\nabla} \times \mathbf{B}) \times \mathbf{B}}{p + \rho} \,, \tag{32}$$

where τ_d is the response or drag time. Assuming Gaussian closure and performing the relevant Wick contractions following Campanelli this generalizes Eq. (6) to

$$\begin{aligned} \partial_t M_k &= -2\eta_{\rm eff} k^2 M_k + \frac{\alpha_+}{4\pi} k^2 H_k \,, \\ \partial_t H_k &= -2\eta_{\rm eff} k^2 H_k + 16\pi\alpha_- M_k \,, \end{aligned} \tag{33}$$

where

$$\begin{aligned} \eta_{\rm eff} &= \eta + \frac{4}{3}\tau_d \frac{U_B/V}{p+\rho} \\ \alpha_\pm &= \frac{2\eta e^2 \mu_5}{\pi} \mp \frac{1}{6} \frac{\tau_d}{p+\rho} \int d\ln k k^2 \frac{H_k}{V} \,, \end{aligned} \tag{34}$$

with V the volume of the system, see also Ref. [17].

However, Eq. (34) only holds for unpolarized magnetic fields, whereas in the limit of maximally helical fields Eq. (32) vanishes ! Thus Eqs. (33) are only applicable if the chiral effect is sub-dominant.

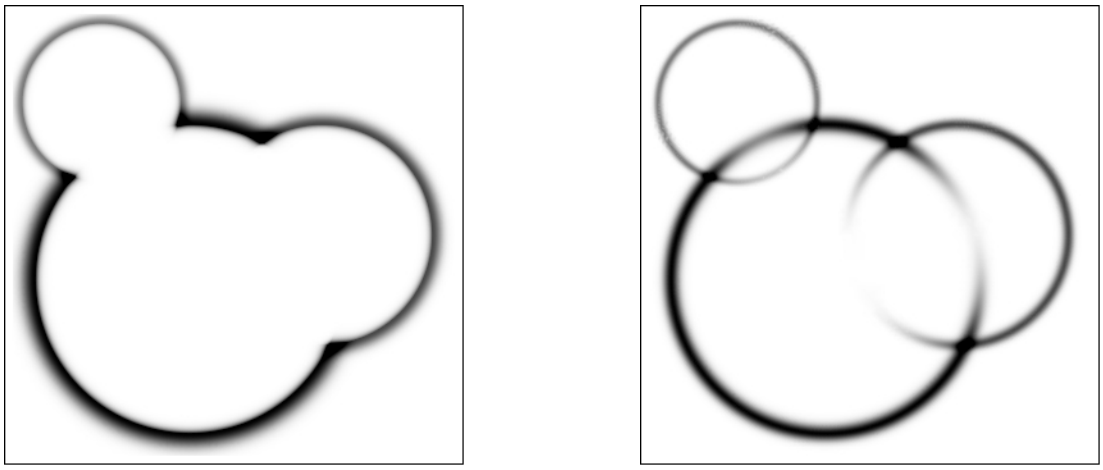

Figure 2: The plots show two sketches of the energy distribution in the envelope (left) and bulk flow (right) approximations. Figures reprinted from Ref. [18]. © 2018 IOP Publishing Ltd and Sissa Medialab.

5 Gravitational waves from hydrodynamics at cosmological phase transitions

One of the most intriguing links between cosmological phase transitions and particle physics are gravitational waves. In case a cosmological phase transition is 1st order, the nucleated bubbles expand and collide towards the end of the phase transition. The latent heat is thereby transformed into kinetic motion of the Higgs field and the plasma. In case the latent heat makes a sizeable fraction of the total energy of the plasma, this can lead to gravitational wave production that is potentially observable with space-based laser interferometers. To assess this effect in the context of the LISA mission is part of the cosmology working group. Several members of C10 are actively involved in this programme [19].

Several effects contribute hereby to the final gravitational wave spectrum. This includes the kinetic energy in the Higgs field itself and the kinetic energy in the plasma. The latter has contributions from sound waves as well as from turbulent motion. The dynamics of the plasma is very rich and in state-of-the-art calculations, the plasma is simulated on a lattice and evolved numerically using a computer cluster. However, also these simulations have technical limitations. Simplified models can overcome these limitations and eventually allow a better understanding of the gravitational wave production. In Ref. [18] the gravitational wave production was quantified in two simplified models. The first is the so-called envelope approximation that dates back to the first papers on the topic [20]. The second is a bulk flow model that takes into account the motion of the plasma after the phase transition is completed. Figure2 shows a sketch of the energy distribution in the two approximations. Due to the simplicity of the model, the resulting GW spectrum can be easily expressed as a function of the characteristics of the phase transition. Figure 3 shows the resulting GW spectrum in the bulk flow model.

Also for the production of GW radiation, model building is an important activity. In particular, it is interesting to assess to what extent models that are appealing due to other

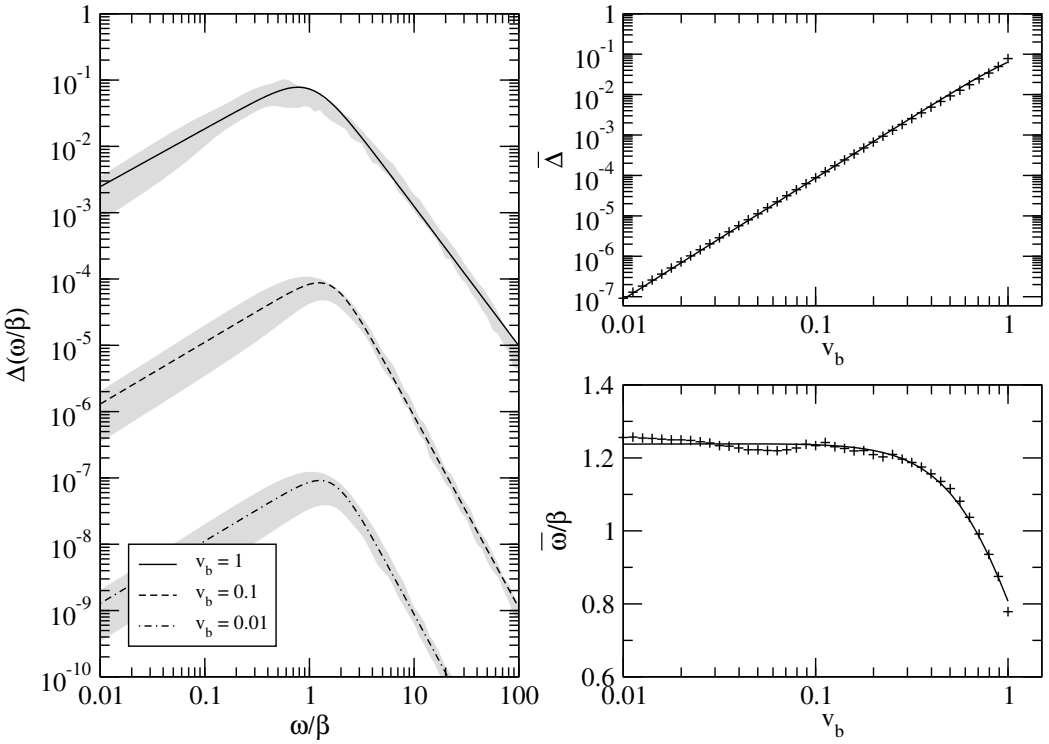

Figure 3: The spectrum of GW as produced by the fluid model. The dependence on the characteristics of the phase transition is almost trivial and can be obtained by rescaling. Figures reprinted from Ref. [18]. © 2018 IOP Publishing Ltd and Sissa Medialab.

model building aspects (e.g. dark matter, baryogenesis, ...) can lead to observable GW signals. One such study was presented in [12] in a singlet extension of the minimal supersymmetric Standard Model that is known to facilitate a good dark matter candidate and electroweak baryogenesis.

In Ref. [21] we calculated the spectrum of gravitational waves originating from a 1st-order phase transition in the primordial cosmological plasma due to magnetohydrodynamic fluctuations. There, we included for the first time the "sweeping effect", which dominates the decorrelation of hydrodynamic fluctuations in turbulent flows. This effect leads to a significant reduction of the gravitational wave spectrum in comparison to previous studies. Moreover, we find that the shape of the spectrum itself depends on the maximal amplitude of the turbulent spectrum and at frequencies larger than the peak frequency the spectrum generally follows a broken power law. This is in contrast to previous studies which considered simple power laws for the limiting case of very small or very large energy scales. We also studied the impact of magnetic helicity on the spectrum and find, in qualitative agreements with previous studies, that magnetic helicity leads to an increase of the gravitational wave spectral energy density at smaller frequencies. Furthermore, we investigated the gravitational wave spectrum caused by compressible turbulence. For the first time, we studied the resulting spectrum in the unified picture of purely compressible (sound waves) and incompressible modes. Until now, these two

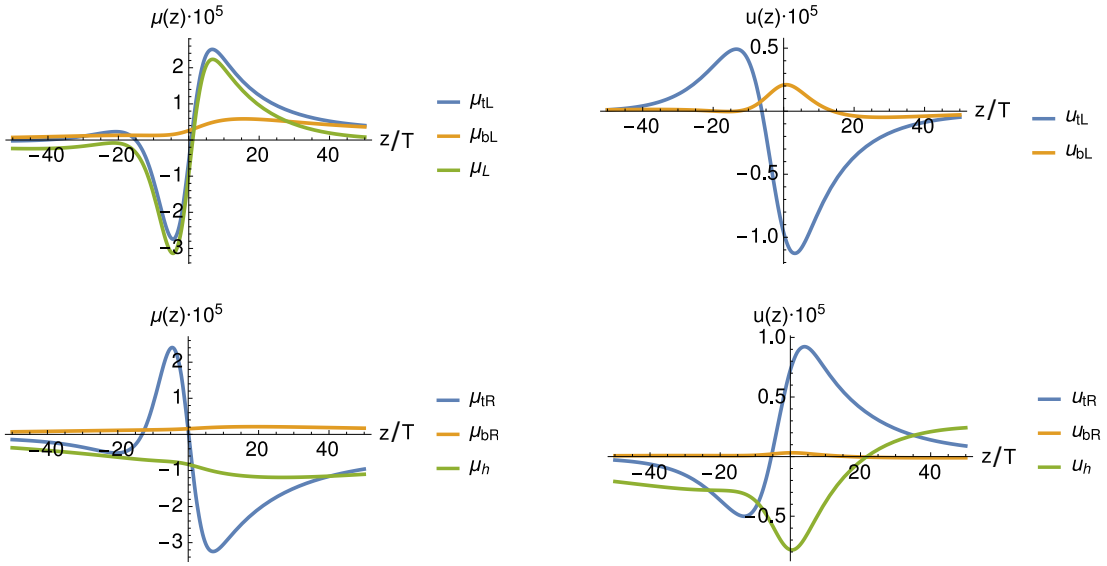

Figure 4: Chemical potentials μ (left) and velocity fields u (right) induced by a varying complex Top quark Yukawa coupling. The upper graphs show the left-handed particle species (and the total left-handed chemical potential) while the lower graphs show the right-handed species and the Higgs. Figures reprinted from Ref. [22]. © 2017 IOP Publishing Ltd and Sissa Medialab.

source terms have been treated independently. Ultimately, we find that the "sweeping effect" due to incompressible modes affects the spectrum driven by purely compressible modes, even if compressible modes are dominant. This leads to a flatter high frequency spectrum and an overall reduced peak amplitude of the gravitational wave spectrum.

6 Electroweak baryogenesis

Any baryogenesis mechanism aims at explaining the apparent disparity between matter and anti-matter. The required ingredients for such a mechanism are a violation of charge and charge-parity conjugation as well as a non-equilibrium situation. The latter ingredients makes a 1st-order cosmological phase transition an interesting target. The resulting baryogenesis mechanism is called electroweak baryogenesis [23].

Since electroweak baryogenesis is based on the non-equilibrium nature of the plasma during the phase transition, it has to be assessed in a framework that can handle genuine quantum effects (CP violation) away from equilibrium. Nowadays, this is achieved using the Schwinger–Keldysh formalism which is an out-of-equilibrium formulation of quantum field theory. In the context of electroweak baryogenesis, the resulting equations are often called quantum (or semi-classical) transport equations (for a review on the topic see [24]).

These quantum transport equations are specific to the model at hand. For example, in the case of Froggatt–Nielsen models mentioned earlier, the Yukawa couplings vary during the phase transition what leads to a very rich phenomenology and new effects in baryogenesis [22].

Figure 4 shows the chemical potentials and the bulk velocity close to the expanding bubbles walls. A mismatch between left- and right- handed chemical potentials is induced by CP-violating interactions in the wall and finally drives the production of the baryon asymmetry.

7 Summary

Cosmological phase transitions of first order have a rich phenomenology and provide many interesting links between cosmology and particle physics. Even though the theoretical foundations are well understood, the field is still in its infancy when it comes to observations. Hopefully, this will change in the near future, with input from particle collider experiments, gravitational wave observatories or a better understanding of magnetic fields in the early Universe.

References

[1] Virgo, LIGO Scientific Collaborations, B. P. Abbott et al., *Observation of Gravitational Waves from a Binary Black Hole Merger*, *Phys. Rev. Lett.* **116** (2016) 061102, [1602.03837].

[2] GROND, SALT Group, OzGrav, DFN, INTEGRAL, Virgo, Insight-Hxmt, MAXI Team, Fermi-LAT, J-GEM, RATIR, IceCube, CAASTRO, LWA, ePESSTO, GRAWITA, RIMAS, SKA South Africa/MeerKAT, H.E.S.S., 1M2H Team, IKI-GW Follow-up, Fermi GBM, Pi of Sky, DWF (Deeper Wider Faster Program), Dark Energy Survey, MASTER, AstroSat Cadmium Zinc Telluride Imager Team, Swift, Pierre Auger, ASKAP, VINROUGE, JAGWAR, Chandra Team at McGill University, TTU-NRAO, GROWTH, AGILE Team, MWA, ATCA, AST3, TOROS, Pan-STARRS, NuSTAR, ATLAS Telescopes, BOOTES, CaltechNRAO, LIGO Scientific, High Time Resolution Universe Survey, Nordic Optical Telescope, Las Cumbres Observatory Group, TZAC Consortium, LOFAR, IPN, DLT40, Texas Tech University, HAWC, ANTARES, KU, Dark Energy Camera GW-EM, CALET, Euro VLBI Team, ALMA, B. P. Abbott et al., *Multi-messenger Observations of a Binary Neutron Star Merger*, *Astrophys. J.* **848** (2017) L12, [1710.05833].

[3] J. R. Espinosa, M. Garny, T. Konstandin and A. Riotto, *Gauge-Independent Scales Related to the Standard Model Vacuum Instability*, *Phys. Rev.* **D95** (2017) 056004, [1608.06765].

[4] R. Jackiw, *Functional evaluation of the effective potential*, *Phys. Rev.* **D9** (1974) 1686.

[5] J. Elias-Miro, J. R. Espinosa and T. Konstandin, *Taming Infrared Divergences in the Effective Potential*, *JHEP* **08** (2014) 034, [1406.2652].

[6] J. R. Espinosa and T. Konstandin, *Resummation of Goldstone Infrared Divergences: A Proof to All Orders*, 1712.08068.

[7] M. Garny and T. Konstandin, *On the gauge dependence of vacuum transitions at finite temperature*, *JHEP* **07** (2012) 189, [1205.3392].

[8] J. R. Espinosa, M. Garny and T. Konstandin, *Interplay of Infrared Divergences and Gauge-Dependence of the Effective Potential*, *Phys. Rev.* **D94** (2016) 055026, [1607.08432].

[9] G. D. Moore and T. Prokopec, *How fast can the wall move? A Study of the electroweak phase transition dynamics*, *Phys. Rev.* **D52** (1995) 7182–7204, [hep-ph/9506475].

[10] T. Konstandin, G. Nardini and I. Rues, *From Boltzmann equations to steady wall velocities*, *JCAP* **1409** (2014) 028, [1407.3132].

[11] G. C. Dorsch, S. J. Huber, T. Konstandin and J. M. No, *A Second Higgs Doublet in the Early Universe: Baryogenesis and Gravitational Waves*, *JCAP* **1705** (2017) 052, [1611.05874].

[12] S. J. Huber, T. Konstandin, G. Nardini and I. Rues, *Detectable Gravitational Waves from Very Strong Phase Transitions in the General NMSSM*, *JCAP* **1603** (2016) 036, [1512.06357].

[13] I. Baldes, T. Konstandin and G. Servant, *A First-Order Electroweak Phase Transition in the Standard Model from Varying Yukawas*, 1604.04526.

[14] P. Pavlović, N. Leite and G. Sigl, *Modified Magnetohydrodynamics Around the Electroweak Transition*, *JCAP* **1606** (2016) 044, [1602.08419].

[15] P. Pavlović, N. Leite and G. Sigl, *Chiral Magnetohydrodynamic Turbulence*, *Phys. Rev.* **D96** (2017) 023504, [1612.07382].

[16] A. Boyarsky, J. Frohlich and O. Ruchayskiy, *Self-consistent evolution of magnetic fields and chiral asymmetry in the early Universe*, *Phys. Rev. Lett.* **108** (2012) 031301, [1109.3350].

[17] M. Dvornikov and V. B. Semikoz, *Influence of the turbulent motion on the chiral magnetic effect in the early Universe*, *Phys. Rev.* **D95** (2017) 043538, [1612.05897].

[18] T. Konstandin, *Gravitational radiation from a bulk flow model*, *JCAP* **1803** (2018) 047, [1712.06869].

[19] C. Caprini et al., *Science with the space-based interferometer eLISA. II: Gravitational waves from cosmological phase transitions*, *JCAP* **1604** (2016) 001, [1512.06239].

[20] A. Kosowsky and M. S. Turner, *Gravitational radiation from colliding vacuum bubbles: envelope approximation to many bubble collisions*, *Phys. Rev.* **D47** (1993) 4372–4391, [astro-ph/9211004].

[21] P. Niksa, M. Schlederer and G. Sigl, *Gravitational Waves produced by Compressible MHD Turbulence from Cosmological Phase Transitions*, *Class. Quant. Grav.* **35** (2018) 144001, [1803.02271].

[22] S. Bruggisser, T. Konstandin and G. Servant, *CP-violation for Electroweak Baryogenesis from Dynamical CKM Matrix*, *JCAP* **1711** (2017) 034, [1706.08534].

[23] V. A. Kuzmin, V. A. Rubakov and M. E. Shaposhnikov, *On the Anomalous Electroweak Baryon Number Nonconservation in the Early Universe*, *Phys. Lett.* **155B** (1985) 36.

[24] T. Konstandin, *Quantum Transport and Electroweak Baryogenesis*, *Phys.Usp.* **56** (2013) 747–771, [1302.6713].